PAPER

Uplink Capacity of OFDM Multi-User MIMO Using Near-ML Detection in a Cellular System

Masashi ITAGAKI[†a)], **Tetsuya YAMAMOTO**[†], **Kazuki TAKEDA**[†], ***Student Members***, *and* **Fumiyuki ADACHI**[†], ***Fellow***

SUMMARY Multi-user multi-input multi-output (MIMO) system has been attracting much attention due to its high spectrum efficiency. Non-linear MIMO signal detection methods with less computational complexity have been widely studied for single-user MIMO systems. In this paper, we investigate how a lattice reduction (LR)-aided detection and a maximum likelihood detection (MLD) employing the QR decomposition and M-algorithm (QRM-MLD), which are commonly known as non-linear MIMO signal detection methods, improve the uplink capacity of a multi-user MIMO-OFDM cellular system, compared to simple linear detection methods such as zero-forcing detection (ZFD) and minimum mean square error detection (MMSED). We show that both LR-aided linear detection and QRM-MLD can achieve higher uplink capacity than simple linear detection at the cost of moderate increase of computational complexity. Furthermore, QRM-MLD can obtain the same uplink capacity as MLD.
key words: *multi-user MIMO, OFDM, lattice reduction, QRM-MLD, uplink capacity*

1. Introduction

High speed data services are strongly demanded in the next generation mobile communication systems. Multi-user multi-input multi-output (MIMO) multiplexing [1], [2] is one of the promising techniques to provide multiple users with high speed data transmission without increasing the signal bandwidth. Uplink multi-user MIMO multiplexing can allow multiple users to simultaneously access the same base station (BS) using the same carrier frequency. The MIMO signal detection needs to recover each users' transmitted signal in a severe multi-user interference (MUI) environment.

There are two types of well-known MIMO signal detection methods, maximum likelihood detection (MLD) and linear detection (such as zero-forcing detection (ZFD) and minimum mean square error detection (MMSED) [3]). MLD has a disadvantage of its prohibitively high computational complexity while linear detection methods have a disadvantage of its poor performance when the number of users is the same as that of receive antennas. Thus, various near-ML detection methods which can provide low bit error rate (BER) with less computational complexity have been widely studied.

In a cellular system, the same frequency is reused in spatially separated different cells to efficiently utilize the limited available spectrum [4] and therefore, the co-channel interference (CCI) limits the link capacity. In [5], the uplink capacity of a multi-user MIMO cellular system is evaluated, but only linear detection methods (i.e., ZFD and MMSED) are considered. How the non-linear MIMO signal detection methods can improve the uplink capacity has not been fully investigated yet.

In this paper, we consider a multi-user MIMO cellular system using orthogonal frequency division multiplexing (OFDM) and investigate, by computer simulation, how non-linear MIMO signal detection methods improve the uplink capacity. Single-user MIMO frequency division multiple access (FDMA) is not considered because the mobile terminal requires multiple antennas. We also discuss the computational complexity. We utilize a lattice reduction (LR)-aided ZFD and MMSED and an MLD employing the QR decomposition and M-algorithm (QRM-MLD). Lattice reduction using Lenstra-Lenstra-Lovasz (LLL) algorithm [6] is considered to be a promising technique to improve the performance of ZFD and MMSED [7], [8]. The advantage of LR-aided ZFD and MMSED is that the full diversity order is obtained if the number of users is lower than or equal to that of receive antennas [9]. QRM-MLD [10] is a computationally efficient near MLD. The search problem is transformed into the tree structured search problem by utilizing the QR decomposition and the computational complexity is reduced by employing the M algorithm.

The remainder of this paper is organized as follows. Section 2 gives the system model. Section 3 presents the OFDM multi-user MIMO uplink transmission system model. In Sect. 4, LR-aided detection and QRM-MLD are described. The simulation results on the uplink capacity are presented in Sect. 5. Section 6 offers some conclusions.

2. System Model

In a cellular system, the same frequency band is reused at different cells to efficiently utilize the limited bandwidth [4]. The number of different OFDM signal bandwidths to cover the entire service area is called the cluster size N. In this paper, we assume that the number of communicating users per cell and that the bandwidth assigned to each cell is the same. Therefore, as the cluster size N gets smaller, the total bandwidth required in the system gets narrower. On the other hand, stronger CCI is received because the co-channel

Manuscript received March 31, 2011.
Manuscript revised August 24, 2011.
[†]The authors are with the Department of Electrical and Communication Engineering, Graduate School of Engineering, Tohoku University, Sendai-shi, 980-8579 Japan.
a) E-mail: masashi@mobile.ecei.tohoku.ac.jp
DOI: 10.1587/transcom.E95.B.198

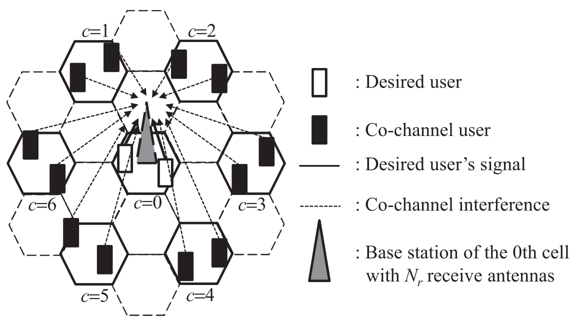

Fig. 1 CCI model of uplink multi-user MIMO in a cellular system when $N = 3$ and $U = 2$.

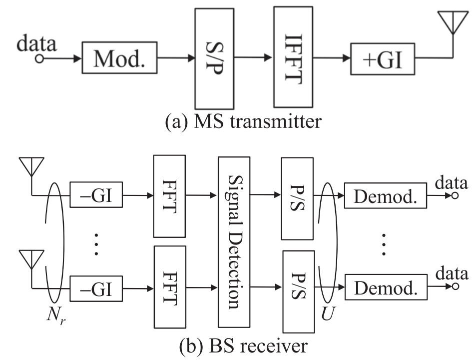

Fig. 2 Transmission system model of OFDM multi-user MIMO.

cells get closer. This suggests that there exists the optimum N that maximizes the uplink capacity.

Figure 1 illustrates the CCI model for the uplink OFDM multi-user MIMO in a cellular system. The number of transmitting users per cell is assumed to be the same for all cells (uniform user distribution) and is denoted by U; i.e., U users in each cell share the same OFDM signal band of N_c subcarriers and each user is simultaneously transmitting its data by using all N_c subcarriers. It is assumed that the BS has N_r ($\geq U$) receive antennas while each user has a single transmit antenna. We consider 6 nearest co-channel cells (i.e., only first-tier co-channel cells) since they are a dominant source of CCI which limits the cellular capacity [11], [12]. The cell of interest is indexed as $c = 0$, and 6 nearest co-channel cells are indexed as $c = 1 \sim 6$.

In this paper, we measure the distribution of local average BER by the Monte-Carlo simulation to find the outage probability of BER [4], [13], which is defined as the probability of the local average BER exceeding the required BER. We define the uplink capacity as the maximum number $U_{\max}$ of supportable users normalized by the cluster size N for the given allowable outage probability Q.

3. OFDM Multi-User MIMO

Figure 2 shows the transmission system model of OFDM multi-user MIMO using N_c subcarriers. At each user terminal transmitter, the binary information sequence is data-modulated and then, the data-modulated symbol sequence is divided into a sequence of blocks of N_c symbols each. The symbol block of u-th user in the c-th cell is represented by $\{\ d_{u(c)}(k)\ ;\ k = 0 \sim N_c - 1\}$. Then, N_c-point inverse fast Fourier transform (IFFT) is applied to generate the time-domain OFDM signal block as

$$s_{u(c)}(t) = \sqrt{\frac{2P}{N_c}} \sum_{k=0}^{N_c-1} d_{u(c)}(k) \exp\left(j2\pi t \frac{k}{N_c}\right), \tag{1}$$

where P is the transmit power and is the same for all users. The last N_g symbols in each block are copied and inserted as a cyclic prefix (CP) into the guard interval (GI) before transmission.

The transmitted OFDM signal block is assumed to go through a frequency-selective block fading channel which is composed of L distinct propagation paths. Assuming the block fading, the path gains stay constant during the transmission of one OFDM signal block. The channel impulse response between the u-th user in the c-th cell and the m-th receive antenna of the c = 0th cell BS is given by

$$h_{m,u(c)}(t) = \sum_{l=0}^{L-1} h_{m,u(c)}(l) \cdot \delta\left(t - \tau_{u(c),l}\right), \tag{2}$$

with

$$h_{m,u(c)}^{(l)} = \sqrt{r_{u(c)}^{-\alpha} \cdot 10^{-\eta_{u(c)}/10}} \cdot g_{m,u(c)}^{(l)}, \tag{3}$$

where $r_{u(c)}$, $\eta_{u(c)}$, and α denote the distance between the user and the c = 0th cell BS, the shadowing loss, and the path-loss exponent, respectively, and $g_{m,u(c)}^{(l)}$ and $\tau_{u(c),l}$ are the complex-valued path gain and the time delay of the l-th path of the u-th user in the c-th cell, respectively, with $E\left[\sum_{l=0}^{L-1} \left|g_{m,u(c)}^{(l)}\right|^2\right] = 1$.

At the c = 0th cell BS, a superposition of U user's transmitted signals as well as CCI is received by N_r receive antennas. The GI-removed received signal block $\mathbf{y}(t) = [y_0(t) \cdots y_{N_r-1}(t)]^T$ can be expressed using the vector form as

$$\mathbf{y}(t) = \sum_{l=0}^{L=1} \mathbf{h}_0^{(l)} \mathbf{s}_0\left((t - \tau_{0,l}) \bmod N_c\right) + \mathbf{i}(t) + \mathbf{n}(t), \tag{4}$$

where $\mathbf{i}(t) = \sum_{c=1}^{6} \sum_{l=0}^{L-1} \mathbf{h}_c^{(l)} \mathbf{s}_c\left(t - \tau_{c,l}\right)$ is an $N_r \times 1$ CCI vector and $\mathbf{n}(t) = \left[n_0(t) \cdots n_{N_r-1}(t)\right]^T$ is an $N_r \times 1$ noise vector, $\mathbf{h}_c^{(l)}$ is an $N_r \times U$ path gain matrix of the l-th path, and $\mathbf{s}_c(t) = \left[s_{0(c)}(t) \cdots s_{U-1(c)}(t)\right]^T$ is a $U \times 1$ transmitted signal vector. The $(m, u(c))$-th element of $\mathbf{h}_c^{(l)}$ is represented by $h_{m,u(c)}^{(l)}$.

The received signal block $\mathbf{y}(t)$ is transformed by N_c-point fast Fourier transform (FFT) into the frequency-domain signal vector $\mathbf{Y}(k) = \left[Y_0(k) \cdots Y_{N_r-1}(k)\right]^T$ as

$$\begin{aligned}\mathbf{Y}(k) &= \frac{1}{\sqrt{N_c}} \sum_{t=0}^{N_c-1} \mathbf{y}(t) \exp\left(-j\frac{2\pi k}{N_c} t\right) \\ &= \mathbf{H}_0(k)\mathbf{S}_0(k) + \mathbf{I}(k) + \mathbf{N}(k), k = 0 \sim N_c - 1,\end{aligned} \tag{5}$$

where $\mathbf{H}_0(k)$ is an $N_r \times U$ channel gain matrix, whose $(m, u(c))$-th element $H_{m,u(c)}(k)$ is given by

$$H_{m,u(c)}(k) = \sqrt{r_{u(c)}^{-\alpha} \cdot 10^{-\eta_{u(c)}/10}} G_{m,u(c)}(k), \tag{6}$$

where

$$G_{m,u(c)}(k) = \sum_{l=0}^{L-1} \exp\left(-j\frac{2\pi k}{N_c}\tau_{u(c),l}\right). \tag{7}$$

Finally, signal detections are carried out using $\mathbf{Y}(k)$.

4. MIMO Signal Detection

We consider ZFD, MMSED, LR aided ZFD, LR aided MMSED, and QRM-MLD as MIMO signal detection methods at the BS. In this section, the frequency index k is omitted for the sake of simplicity.

4.1 ZFD and MMSED [3]

The output of ZFD is given as

$$\mathbf{S}_{0,\mathrm{ZF}} = \left(\mathbf{H}_0^H \mathbf{H}_0\right)^{-1} \mathbf{H}_0^H \mathbf{Y}. \tag{8}$$

The output of MMSED can be written in similar form to ZFD by introducing an $(N_r + U) \times U$ channel gain matrix $\mathbf{H}_{\mathrm{ext}}$ and an $(N_r + U) \times 1$ received signal vector $\mathbf{Y}_{\mathrm{ext}}$ [14]. $\mathbf{H}_{\mathrm{ext}}$ and $\mathbf{Y}_{\mathrm{ext}}$ are given as

$$\mathbf{H}_{\mathrm{ext}} = \begin{bmatrix} \mathbf{H}_0 \\ \sqrt{\frac{\sigma_I^2+\sigma_n^2}{P}}\mathbf{I}_U \end{bmatrix} \text{ and } \mathbf{Y}_{\mathrm{ext}} = \begin{bmatrix} \mathbf{Y}_0 \\ \mathbf{0}_U \end{bmatrix}, \tag{9}$$

where $\mathbf{I}_U$ is an $U \times U$ unit matrix, $\mathbf{0}_U$ is an $U \times 1$ vector whose elements are all 0, and σ_I^2 and σ_n^2 denote the average received CCI power and the noise power, respectively. The output of MMSED can be written as

$$\begin{aligned} \mathbf{S}_{0,\mathrm{MMSE}} &= \left(\mathbf{H}_0^H \mathbf{H}_0 + \frac{\sigma_I^2 + \sigma_n^2}{P}\mathbf{I}_U\right)^{-1} \mathbf{H}_0^H \mathbf{Y} \\ &= \left(\mathbf{H}_{\mathrm{ext}}^H \mathbf{H}_{\mathrm{ext}}\right)^{-1} \mathbf{H}_{\mathrm{ext}}^H \mathbf{Y}_{\mathrm{ext}}. \end{aligned} \tag{10}$$

The use of LR always achieves the full diversity order of N_r [9] while the diversity order of ZFD and MMSED without LR is $N_r - U + 1$ [15].

4.2 LR-ZFD and LR-MMSED [7], [8]

The purpose of introducing the LR is to transform $\mathbf{H}_0$ into a new matrix $\tilde{\mathbf{H}}_0$ consisting of near-orthogonal column vectors. The signal detection using $\tilde{\mathbf{H}}_0$ produces less noise enhancement compared to that using $\mathbf{H}_0$ [8]. In this paper, we realize the LR by using the LLL algorithm [6]. The detail of LLL algorithm is described in detail in Appendix.

At first, we consider LR-ZFD. By applying the LLL algorithm to $\mathbf{H}_0$, we obtain $\tilde{\mathbf{H}}_0 = \mathbf{H}_0\mathbf{T}$, where $\mathbf{T}$ is the $U \times U$ transform matrix. Then, Eq. (5) can be rewritten as

$$\begin{aligned} \mathbf{Y} &= \mathbf{H}_0\mathbf{S}_0 + \mathbf{I} + \mathbf{N} \\ &= \mathbf{H}_0\mathbf{T}\mathbf{T}^{-1}\mathbf{S}_0 + \mathbf{I} + \mathbf{N} \\ &= \tilde{\mathbf{H}}_0\tilde{\mathbf{S}}_0 + \mathbf{I} + \mathbf{N}, \end{aligned} \tag{11}$$

where $\tilde{\mathbf{S}}_0 = \mathbf{T}^{-1}\mathbf{S}_0$ and $\tilde{\mathbf{H}}_0 = \mathbf{H}_0\mathbf{T}$ are the transformed signal vector and equivalent channel matrix, respectively.

The output of LR-ZFD is given as

$$\tilde{\mathbf{S}}_{0,\mathrm{LR-ZF}} = \left(\tilde{\mathbf{H}}_0^H \tilde{\mathbf{H}}_0\right)^{-1} \tilde{\mathbf{H}}_0^H \mathbf{Y}. \tag{12}$$

Hard decision on $\tilde{\mathbf{S}}_{0,\mathrm{LR-ZF}}$ is done first and then, $\mathbf{S}_{0,\mathrm{LR-ZF}}$ is obtained using the relationship $\mathbf{S}_{0,\mathrm{LR-ZF}} = \mathbf{T}\tilde{\mathbf{S}}_{0,\mathrm{LR-ZF}}$.

In the case of LR-MMSED, the LLL algorithm is applied to the channel matrix $\mathbf{H}_{\mathrm{ext}}$ instead of $\mathbf{H}_0$ [8]. Then, we obtain a $U \times U$ transform matrix $\mathbf{T}_{\mathrm{ext}}$. The output of LR-MMSED is expressed as

$$\tilde{\mathbf{S}}_{0,\mathrm{LR-MMSE}} = \left(\tilde{\mathbf{H}}_{\mathrm{ext}}^H \tilde{\mathbf{H}}_{\mathrm{ext}}\right)^{-1} \tilde{\mathbf{H}}_{\mathrm{ext}}^H \mathbf{Y}_{\mathrm{ext}}, \tag{13}$$

where $\tilde{\mathbf{H}}_{\mathrm{ext}} = \mathbf{H}_{\mathrm{ext}}\mathbf{T}_{\mathrm{ext}}$. Similar to LR-ZFD, hard decision on $\tilde{\mathbf{S}}_{0,\mathrm{LR-MMSE}}$ is done first and then, $\mathbf{S}_{0,\mathrm{LR-MMSE}}$ is obtained using the relationship $\mathbf{S}_{0,\mathrm{LR-MMSE}} = \mathbf{T}_{\mathrm{ext}}\tilde{\mathbf{S}}_{0,\mathrm{LR-MMSE}}$.

4.3 QRM-MLD [10]

As a first step of QRM-MLD, QR decomposition is applied to the channel matrix $\mathbf{H}_0$. In this paper, we use the *sorted QR decomposition* (SQRD), proposed in [16], as ordering. By applying SQRD to the matrix $\mathbf{H}_0$, we obtain the following relationship

$$\mathbf{H}_0 = \mathbf{QRP}, \tag{14}$$

where $\mathbf{Q}$ is an $N_r \times U$ matrix satisfying $\mathbf{Q}^H\mathbf{Q} = \mathbf{I}_U$ and $\mathbf{R}$ is a $U \times U$ upper triangular matrix given as

$$\mathbf{R} = \begin{bmatrix} R_{0,0} & R_{0,1} & \cdots & R_{0,U-1} \\ & R_{1,1} & \cdots & R_{1,U-1} \\ & & \ddots & \vdots \\ \mathbf{0} & & & R_{U-1,U-1} \end{bmatrix}. \tag{15}$$

$\mathbf{P}$ is a $U \times U$ permutation matrix. Since column vectors of $\mathbf{H}_0$ can be interchanged by SQRD, the permutation matrix $\mathbf{P}$ is required. In this section, we assume that $\mathbf{P}$ is a $U \times U$ unit matrix for the sake of simplicity.

Next, the received signal vector $\mathbf{Y}$ is transformed into $\hat{\mathbf{Y}}$ as

$$\begin{aligned} \hat{\mathbf{Y}} &= \left[\hat{Y}_0 \cdots \hat{Y}_{U-1}\right]^T \\ &= \mathbf{Q}^H\mathbf{Y} \\ &= \sqrt{2P}\begin{bmatrix} R_{0,0} & \cdots & R_{0,U-1} \\ & \ddots & \vdots \\ \mathbf{0} & & R_{U-1,U-1} \end{bmatrix} \begin{bmatrix} S_{0(0)} \\ \vdots \\ S_{U-1(0)} \end{bmatrix} \\ &\quad + \mathbf{Q}^H\mathbf{I} + \mathbf{Q}^H\mathbf{N}. \end{aligned} \tag{16}$$

Then, the M algorithm [17], which consists of U stages, is

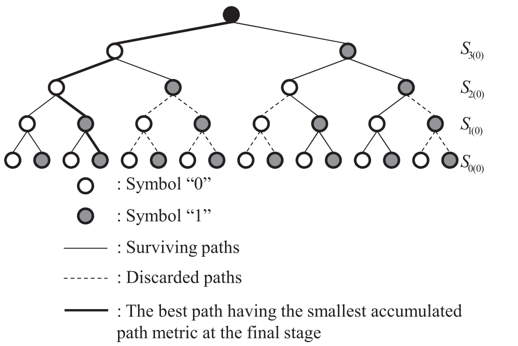

Fig. 3 An example of QRM-MLD (BPSK, $U = 4$, and $M = 4$).

applied to the vector $\hat{\mathbf{Y}}$. In each stage, the accumulated path metric using the squared Euclidian distance between $\hat{\mathbf{Y}}$ and a path arriving at each node is calculated and then, M paths having the smallest accumulated path metric are selected as surviving paths. The accumulated path metric in the k-th stage is given as

$$e_k = \sum_{n=0}^{k-1} \left| \hat{Y}_{U-1-n} - \sqrt{2P} \sum_{i=0}^{n} R_{U-1-n,U-1-i} \bar{S}_{U-1-i(0)} \right|^2 \quad (k = 1 \sim U), \qquad (17)$$

where $\bar{S}_{U-1-i(0)}$ is a symbol candidate for $S_{U-1-i(0)}$. At the U-th stage (which is the final stage), the best path having the smallest accumulated path metric is chosen. The best path is traced back to output the detected signal vector. A brief example of QRM-MLD assuming BPSK modulation, $U = 4$, and $M = 4$ is illustrated in Fig. 3.

5. Computer Simulation

5.1 Simulation Procedure

Table 1 shows the simulation condition. The channel is assumed to be a frequency-selective block Rayleigh fading having a symbol-spaced L-path uniform power delay profile (i.e., $E\left[\left|g_{m,u(c)}^{(l)}\right|^2\right] = 1/L$ for $l = 0 \sim L-1$). Unless otherwise stated, the cell radius is normalized to unity and the transmit power P is set so that the average received bit energy-to-noise power spectrum density ratio E_b/N_0 measured at a distance equal to the cell radius becomes 10 dB (this is called the normalized transmit E_b/N_0 in this paper). Ideal channel estimation is assumed.

It is shown in [5] that in a strong frequency-selective fading channel, both the slow and fast transmit power control (TPC) provide almost the same maximum uplink capacity and therefore, the slow TPC can be used. However, Ref. [5] also shows that the maximum uplink capacity achievable by the slow TPC is almost the same as that without TPC. Therefore, in this paper, the TPC is not considered.

Figure 4 illustrates the computer simulation procedure. First, U users' locations are randomly generated in each cell for the given cluster size N. Next, the path-loss and the log-normally distributed shadowing loss are generated for each user. Then, an L-path block Rayleigh fading associated with each user is generated. The signal transmission is simulated to measure the local average BERs of U users in the $c = 0$th cell. This BER measurement is repeated a sufficient number of times by randomly changing the user locations, path-loss, shadowing loss, and fading in order to obtain the complementary cumulative distribution function (CCDF) of the local average BER. The outage probability is defined as the probability that the local average BER exceeds the required BER. If the outage probability is less than the allowable outage probability Q, the number U of users is incremented by one.

The spectrum efficiency of a cellular system increases as the number of communicating users per cell increases for the given total bandwidth (or the given total number of channels). In this paper, assuming the same data rate for all users, the maximum number $U_{\max}$ of supportable users per cell normalized by the cluster size N is defined as the uplink capacity. The reason to normalize the maximum number of supportable users by the cluster size is that as the cluster size

Table 1 Simulation condition.

Transmitter	Data modulation	QPSK
	Number of users per cell	$U(\leq N_r)$
	Number of subcarriers	$N_c = 64$
	GI length	$N_g = 16$
	Normalized transmit E_b/N_0	$10, \infty$(dB)
Channel	Fading type	Frequency selective block Rayleigh
	Power delay profile	$L = 16$-path uniform
	Path-loss exponent	$\alpha = 3.5$
	Standard deviation of shadowing loss	$\sigma = 7.0$(dB)
	Cluster size	$N = 1 \sim 25$
Receiver	Number of receive antennas	$N_r = 4, 6, 8$
	Channel estimation	Ideal
	LLL parameter	$\delta = 0.75$
	Number of surviving pahts	$M = 1, 4$
Required quality	Required BER	10^{-3}
	Allowable outage probability	$Q = 0.1$

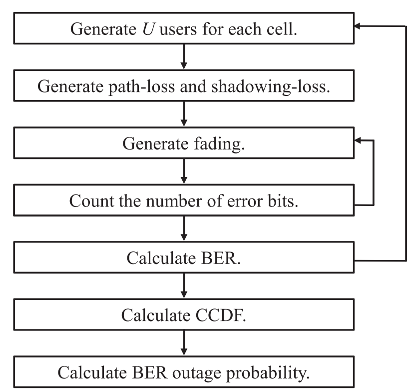

Fig. 4 Computer simulation procedure.

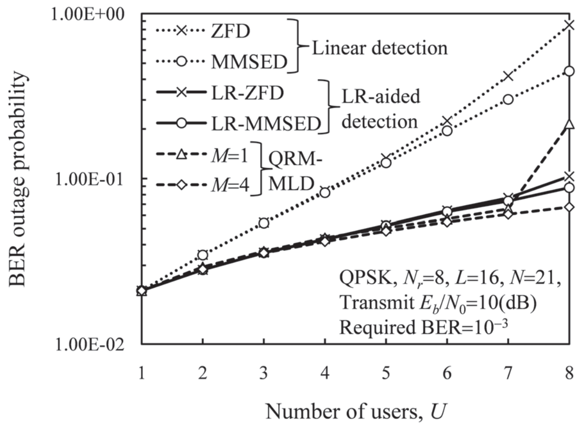

Fig. 5 Outage probability.

increases, the total bandwidth (or the total number of channels) increases. The uplink capacity depends on the modulation level and the error correcting code. In this paper, we set the required BER and the allowable outage probability as BER $= 10^{-3}$ and $Q = 0.1$, respectively.

5.2 Uplink Capacity

Figure 5 illustrates the BER outage probability as a function of the number U of users per cell when $N_r = 8$ and $N = 21$. It can be seen from Fig. 5 that using conventional ZFD and MMSED, the outage probability significantly increases with U since their diversity order is $N_r - U + 1$. Much lower outage probability is achieved with LR-aided detection compared to conventional ZFD and MMSED. This is because the diversity order is always N_r for both LR-ZFD and LR-MMSED. QRM-MLD achieves slightly lower outage probability than LR-aided detection. This is because QRM-MLD eliminates the MUI perfectly if the correct path is selected while the MUI still remains in the output of LR-aided detection (each column vector of $\tilde{\mathbf{H}}_0$ or $\tilde{\mathbf{H}}_{\mathrm{ext}}$ are not orthogonal (near orthogonal)). However, when $U = N_r$ and $M = 1$, the BER outage probability of QRM-MLD significantly increases. If U is smaller than N_r, the receive antenna diversity can be obtained and therefore, lower outage probability is achieved even if $M = 1$ is used (only single path is selected in each stage of M algorithm). When $U = N_r$, however, no receive antenna diversity is achieved and the diagonal elements of matrix $\mathbf{R}$ often drop; in particular, $|R_{U-1,U-1}|$ drops significantly [18]. Accordingly, the probability of discarding the correct path increases. Therefore, to avoid this problem, $M = 4$ must be used when $U = N_r$.

Figure 6 plots the uplink capacity $U_{\max}/N$ as a function of the cluster size N when $N_r = 8$. Also plotted is the performance of MLD for a comparison. The value of $U_{\max}$ is also indicated near each plot in the figure. First, we discuss how the introduction of lattice reduction (LR) into ZFD and MMSED improves their uplink capacities. It is clearly seen from Fig. 6(a) that the introduction of LR can significantly improve the capacity (note that the conventional ZFD and MMSED provide the same uplink capacity, however, LR-

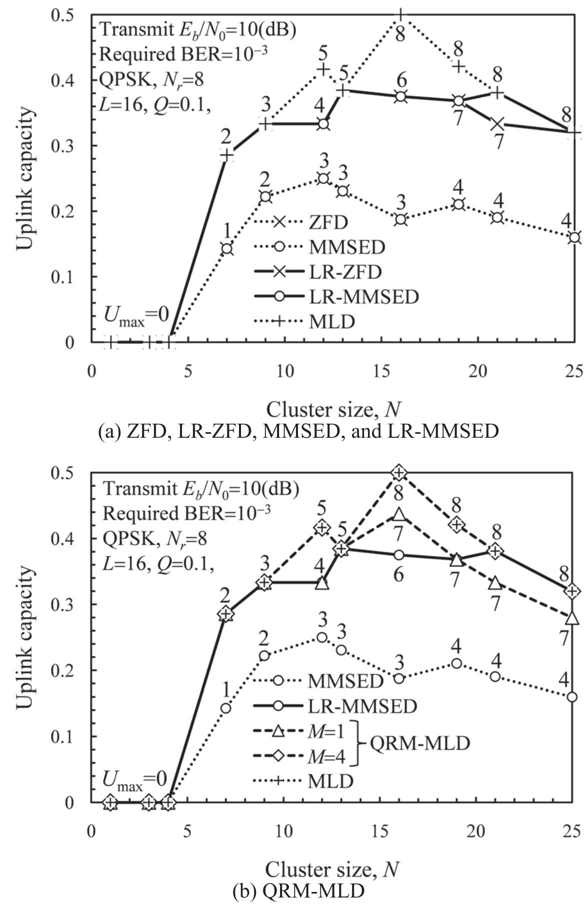

Fig. 6 Uplink capacity.

ZFD and LR-MMSED provide almost the same improved uplink capacity). Next, we discuss how better QRM-MLD performs than LR-MMSED. It can be seen from Fig. 6(b) that when $M = 4$, QRM-MLD can achieve the same uplink capacity as MLD, unlike LR-MMSED (however, note that when $M = 1$, QRM-MLD provides smaller capacity than LR-MMSED for a large N).

5.3 Computational Complexity

The trade-off relationship between the maximum uplink capacity and the computational complexity is discussed in the case of $N_r = 8$. In this paper, the computational complexity is defined as the number of complex multiplications and additions per block. The number of multiplications and additions is shown in Table 2 for each detection method. We measure the complexity of LLL algorithm by computer simulation since it depends on the channel condition. In Table 2, X denotes the modulation level and is 4 in this paper since we consider QPSK modulation.

The approximate values of the number of complex multiplications and additions per block required to achieve the maximum uplink capacity are summarized for each detection method in Table 3. LR-MMSED achieves about 1.54 times higher maximum capacity at the cost of about 7.4 and 7.3 times increased number of complex multiplications and

Table 2 Number of complex multiplications and additions per block.

-	Multiplications		
-	MMSED	LR-MMSED	QRM-MLD
Detection of $\mathbf{S}_{0,\mathrm{MMSE}}$	$N_c\left\{U^3 + 2N_rU^2 + N_rU\right\}$	-	-
MMSE SQRD [14]	-	$N_c\left\{U^2(N_r + U) + (U/2)(U-1)\right\}$	-
Calculation of $\mathbf{T}^{-1}$	-	N_cU^3	-
Detection of $\tilde{\mathbf{S}}_{0,\mathrm{LR-MMSE}}$	-	$N_c\left\{U^3 + 2(N_r + U)U^2 + (N_r + U)U\right\}$	-
Detection of $\mathbf{S}_{0,\mathrm{LR-MMSE}}$	-	N_cU^2	-
SQRD [16]	-	-	$(1/2)N_cUN_r(3U-1)$
Calculation of $\hat{\mathbf{Y}}$	-	-	N_cN_rU
Calculation of squared Euclidian distance	-	-	$N_cX\{2 + (M/2)(U+4)(U-1)\}$
-	Additions		
-	MMSED	LR-MMSED	QRM-MLD
Detection of $\mathbf{S}_{0,\mathrm{MMSE}}$	$N_c\left\{U^3 + 2N_rU^2 + U(N_r-1)\right\}$	-	-
MMSE SQRD [14]	-	$N_c\left\{U^2(N_r + U) - U-)\right\}$	-
Calculation of $\mathbf{T}^{-1}$	-	$N_c(U^3 + U^2 + U)$	-
Detection of $\tilde{\mathbf{S}}_{0,\mathrm{LR-MMSE}}$	-	$N_c\left\{U^3 + 2(N_r + U)U^2 + (N_r + U - 1)U\right\}$	-
Detection of $\mathbf{S}_{0,\mathrm{LR-MMSE}}$	-	$N_cU(U-1)$	-
SQRD [16]	-	-	$(1/2)N_cUN_r(3U-1) - U^3$
Calculation of $\hat{\mathbf{Y}}$	-	-	$N_cU(N_r-1)$
Calculation of squared Euclidian distance	-	-	$N_cX\{1 + (M/2)(U+4)(U-1)\}$

Table 3 Maximum uplink capacity and computational complexity comparison in the case of $N_r = 8$.

Detection method	Maximum uplink capacity	No. of complex multiplications	No. of complex additions
MMSED	$0.25(U=3)$	1.2×10^4	1.2×10^4
LR-MMSED	$0.38(U=5)$	8.9×10^4	8.8×10^4
QRM-MLD($M=1$)	$0.44(U=7)$	4.8×10^4	4.8×10^4
QRM-MLD($M=4$)	$0.50(U=8)$	9.5×10^4	9.3×10^4

additions, respectively, compared to MMSED. Furthermore, it can be seen that QRM-MLD achieves 1.75 (2.0) times higher maximum capacity at the cost of about 4.0 (7.9) and 4.0 (8.2) times increased number of multiplications and additions, respectively, compared to MMSED in the case of $M = 1$ (4).

Both LR-MMSED and QRM-MLD provides larger maximum uplink capacity at a moderate increase in the computational complexity. Furthermore, when $M = 1$, QRM-MLD can achieve larger maximum uplink capacity with less computational complexity compared to LR-MMSED. If the value of M is set to 4, QRM-MLD achieves larger maximum uplink capacity compared to LR-MMSED at the cost of slightly higher complexity. However, we note that QRM-MLD has a disadvantage that its complexity depends on the modulation level unlike LR-MMSED.

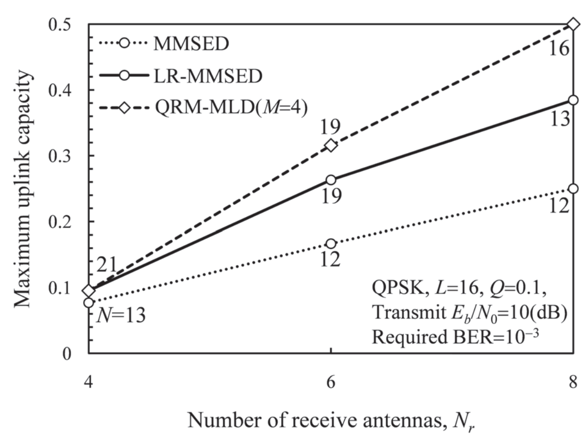

Fig. 7 Maximum uplink capacity.

5.4 Impact of Parameters

Figure 7 plots the maximum uplink capacity as a function of the number of receive antennas, N_r, for conventional MMSED, LR-MMSED, and QRM-MLD. The value of N is also indicated near each plot in the figure. It can be seen from the figure that by increasing N_r, the advantage of LR-MMSED and QRM-MLD over MMSED can be much pronounced. This is because LR-MMSED and QRM-MLD achieve increasing diversity order as the number of receive antennas increases.

Figure 8 plots the uplink capacity for an interference limited channel (i.e., the transmit $E_b/N_0 \to \infty$). Capacity comparison between the cases of interference-limited condition (Fig. 8) and power-limited condition (Fig. 6) shows that the uplink capacity increases as the transmit power increases, but the value of N which maximizes the uplink capacity is relatively large (i.e., when $N = 13, 16$). This implies that the multi-user MIMO signal detection is very sen-

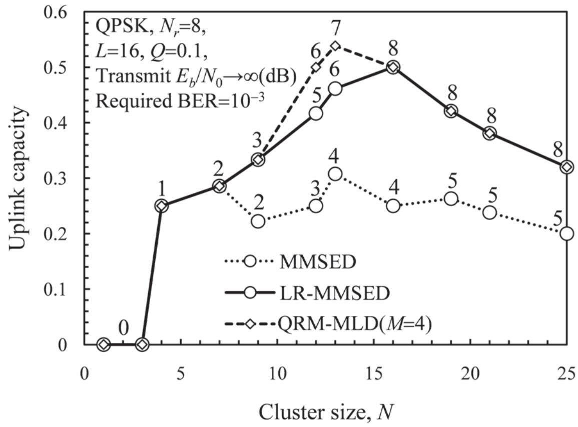

Fig. 8 Uplink capacity (normalized transmit $E_b/N_0 \to \infty$).

sitive to the uncontrollable CCI similar to with the single-user MIMO.

6. Conclusion

We investigated the uplink capacity of OFDM multi-user MIMO using near-ML detection in a cellular system by computer simulation. What we showed in this paper is summarized below. Both LR-aided detection and QRM-MLD can provide much lower outage probability and hence, can achieve higher uplink capacity than ZFD and MMSED. QRM-MLD($M = 4$) achieves the same uplink capacity as MLD unlike LR-MMSED. We also considered the trade-off relationship between the achievable uplink capacity and computational complexity. Both LR aided detection and QRM-MLD achieve higher uplink capacity at the cost of about 4 $\sim$ 8 times increased complexity compared to MMSED. As the number of receive antennas increases, the achievable diversity order of LR aided detection and QRM-MLD increases and hence, their advantage over MMSED becomes more pronounced.

In this paper, we assumed that all users in each cell are communicating simultaneously with their corresponding BS. However, an introduction of a scheduling algorithm which chooses some users having better channel condition can improve the uplink capacity through the multi-user diversity. The link capacity investigation of a cellular system using the multi-user MIMO and scheduling is left as an important future study.

From the simulation results shown in the paper, the cluster size which maximizes the uplink capacity was found to be relatively large. This is because the multi-user MIMO is very sensitive to the CCI and the transmission performance of a user near the cell edge degrades significantly due to the strong CCI. The reuse partitioning [19] (where the single frequency reuse is used in an area near the BS while the conventional frequency reuse is used in an area near the cell edge) can improve the spectrum efficiency of cellular systems. Our simulation results suggest that in a cellular system using reuse partitioning, the multi-user MIMO can be applied for users near the BS while antenna diversity is applied for users near the cell edge. The link capacity investigation of a cellular system using reuse partitioning, multi-user MIMO, and antenna diversity is also left as an important future study.

References

[1] Q.H. Spencer, C.B. Peel, A.L. Swindlehurst, and M. Haardt, “An introduction to the multi-user MIMO downlink,” IEEE Commun. Mag., vol.42, no.10, pp.60–67, Oct. 2004.
[2] S. Sfar, R.D. Murch, and K.B. Letaief, “Layered space-time multiuser detection over wireless uplink systems,” IEEE Trans. Wireless Commun., vol.2, no.4, pp.653–668, July 2003.
[3] E. Biglieri, R. Calderbank, A. Constantinides, A. Goldsmith, A. Paulraj, and H. Vincent Poor, MIMO Wireless Communications, Cambridge University Press, 2007.
[4] W.C. Jakes, Jr., ed., Microwave mobile communications, John Wiley & Sons, New York, 1974.
[5] T. Chiba, Kazuaki Takeda, Kazuki Takeda, and F. Adachi, “Uplink capacity of a cellular system using multi-user single-carrier MIMO multiplexing combined with frequency-domain equalization and transmit power control,” Wireless Personal Communications, doi:10.1007/s11277-010-0130-5, Sept. 2010.
[6] A.K. Lenstra, H.W. Lenstra, Jr., and L. Lovasz, “Factoring polynomials with rational coefficients,” Math. Ann., vol.261, pp.515–534, 1982.
[7] H. Yao and G. Wornell, “Lattice-reduction-aided detectors for MIMO communication systems,” IEEE Proc. Globecom, Taipei, Taiwan, Nov. 2002.
[8] D. Wübben, R. Böhnke, V. Kühn, and K.D. Kammeyer, “Near-maximum-likelihood detection of MIMO systems using MMSE-based lattice-reduction,” IEEE Proc. International Conference on Communications (ICC), pp.798–802, Paris, France, June 2004.
[9] M. Taherzadeh, A. Mobasher, and A.K. Khandani, “LLL reduction achieves the receive diversity in MIMO decoding,” IEEE Trans. Inf. Theory, vol.53, no.12, pp.4801–4805, Dec. 2007.
[10] L.J. Kim and J. Yue, “Joint channel estimation and data detection algorithms for MIMO-OFDM systems,” Proc. Thirty-Sixth Asilomar Conference on Signals, System and Computers, pp.1857–1861, Nov. 2002.
[11] H. Bao and J. Liu, “A novel inter-cell interference coordination scheme for OFDMA system,” Proc. 2010 IEEE International Conference on Intelligent Computing and Intelligent Systems (ICIS), vol.2, p.312, Oct. 2010.
[12] S.D. Roy and S. Kundu, “Outage analysis in presence of correlated interferers in a cognitive-cellular network,” Proc. 2010 IEEE Symposium on Industrial Electronics & Applications (ISIEA), p.100, Oct. 2010.
[13] A. Goldsmith, Wireless communications, Cambridge University Press, New York, 2006.
[14] D. Wübben, R. Böhnke, V. Kühn, and K.D. Kammeyer, “MMSE extension of V-BLAST based on sorted QR decomposition,” Proc. IEEE Vehicular Technology Conference (VTC), vol.1, no.58, pp.508–512, Oct. 2003.
[15] J.H. Winters, J. Salz, and R.D. Gitlin, “The impact of antenna diversity on the capacity of wireless communication systems,” IEEE Trans. Commun., vol.42, no.2/3/4, pp.1740–1751, Feb./March/April 1994.
[16] D. Wübben, R. Böhnke, J. Rinas, V. Kühn, and K.D. Kammeyer, “Efficient algorithm for decoding layered space-time codes,” Electron. Lett., vol.37, no.22, pp.1348–1350, Oct. 2001.
[17] J.B. Anderson and S. Mohan, “Sequential coding algorithms: A survey and cost analysis,” IEEE Trans. Commun., vol.32, pp.169–176, Feb. 1984.
[18] T. Yamamoto, K. Takeda, and F. Adachi, “Single-carrier transmission using QRM-MLD with antenna diversity,” Proc. The 12th In-

ternational Symposium on Wireless Personal Multimedia Communications (WPMC2009), Sendai, Japan, Sept. 2009.
[19] S.W. Halpern, “Reuse partitioning in cellular systems,” Proc. IEEE Vehicular Technology Conference (VTC), pp.322–327, May 1983.
[20] M. Sandell, A. Lillie, D. McNamara, V. Ponnampalam, and D. Milford, “Complexity study of lattice reduction for MIMO detection,” Proc. IEEE WCNC, March 2007.

Appendix: LLL Algorithm

The lattice of matrix $\mathbf{H}_0 = [\mathbf{H}_{0,0} \cdots \mathbf{H}_{0,U-1}]$ is defined as

$$\begin{aligned} L(\mathbf{H}_0) &= L(\mathbf{H}_{0,0}, \cdots, \mathbf{H}_{0,U-1}) \\ &= \sum_{k=0}^{U-1} x\mathbf{H}_k,\ x \in \mathbf{Z}, \end{aligned} \tag{A$\cdot$1}$$

where $\mathbf{H}_{0,0}, \cdots, \mathbf{H}_{0,U-1}$ are column vectors of matrix $\mathbf{H}_0$ and called the lattice basis, and $\mathbf{Z}$ represents the infinite integer space [6].

The LLL algorithm [6] is one of the methods to perform the lattice reduction. Firstly, QR decomposition is applied to obtain $\mathbf{H}_0 = \mathbf{QR}$, where $\mathbf{Q}$ is an $N_r \times U$ matrix which satisfies $\mathbf{Q}^H\mathbf{Q} = \mathbf{I}_U$ and $\mathbf{R}$ is a $U \times U$ upper triangular matrix. In this paper, we use the *sorted QR decomposition* which was proposed in [16]. This algorithm is expanded to the MMSE based signal detection (i.e., $\mathbf{H}_{\text{ext}}$) in [14]. By the use of sorted QR decomposition, the computational complexity of LLL algorithm can be reduced [8].

The inputs to the LLL algorithm are $\mathbf{Q}$ and $\mathbf{R}$, and its outputs are $\tilde{\mathbf{Q}}$ of size $N_r \times U$, $\tilde{\mathbf{R}}$ of size $U \times U$, and $\mathbf{T}$ of size $U \times U$. $\mathbf{T}$ is a unimodular matrix [8], which consists of only Gaussian integer and its determinant is 1 or −1. The lattice reduced matrix $\tilde{\mathbf{H}}_0$ is given as [8]

$$\tilde{\mathbf{H}}_0 = \mathbf{H}_0\mathbf{T}. \tag{A$\cdot$2}$$

Elements of $\tilde{\mathbf{R}}$ satisfy the following two conditions:

$$\left|\tilde{R}_{l,k}\right| \le \frac{1}{2}\left|\tilde{R}_{l,l}\right| \qquad (0 \le l < k \le U-1), \tag{A$\cdot$3}$$

$$\begin{aligned} \delta\left|\tilde{R}_{k-1,k-1}\right|^2 &\le \left|\tilde{R}_{k,k}\right|^2 + \left|\tilde{R}_{k-1,k}\right|^2 \\ &\qquad (k = 1, \cdots, U-1). \end{aligned} \tag{A$\cdot$4}$$

The range of δ is $1/4 < \delta \le 1$ [6]. Since $\delta = 3/4$ is often used [6], [8], [19], $\delta = 3/4$ is also used in Sect. 5 of this paper.

Masashi Itagaki received his B.S. degree in Electrical, Information and Physics Engineering from Tohoku University, Sendai, Japan, in 2009. Currently he is a graduate student at the Department of Electrical and Communications Engineering, Tohoku University. His research interests include multi-user MIMO in cellular systems.

Tetsuya Yamamoto received his B.S. degree in Electrical, Information and Physics Engineering in 2008 and M.S. degree in communications engineering, in 2010, respectively, from Tohoku University, Sendai, Japan. Currently, he is a Japan Society for the Promotion of Science (JSPS) research fellow, studying toward his PhD degree at the Department of Electrical and Communications Engineering, Graduate School of Engineering, Tohoku University. His research interests include frequency-domain equalization and signal detection techniques for mobile communication systems. He was a recipient of the 2008 IEICE RCS (Radio Communication Systems) Active Research Award.

Kazuki Takeda received his B.S., M.S., and Dr. Eng. degrees in communications engineering from Tohoku University, Sendai, Japan, in 2006, 2008, and 2010, respectively. From April 2008 to March 2011, he was a Japan Society for the Promotion of Science (JSPS) research fellow. Since April 2011, he has been with Panasonic Corporation. He was a recipient of the 2009 IEICE RCS (Radio Communication Systems) Active Research Award.

Fumiyuki Adachi received the B.S. and Dr. Eng. degrees in electrical engineering from Tohoku University, Sendai, Japan, in 1973 and 1984, respectively. In April 1973, he joined the Electrical Communications Laboratories of Nippon Telegraph & Telephone Corporation (now NTT) and conducted various types of research related to digital cellular mobile communications. From July 1992 to December 1999, he was with NTT Mobile Communications Network, Inc. (now NTT DoCoMo, Inc.), where he led a research group on wideband/broadband CDMA wireless access for IMT-2000 and beyond. Since January 2000, he has been with Tohoku University, Sendai, Japan, where he is a Professor of Electrical and Communication Engineering at the Graduate School of Engineering. His research interests are in CDMA wireless access techniques, equalization, transmit/receive antenna diversity, MIMO, adaptive transmission, and channel coding, with particular application to broadband wireless communications systems. He is a program leader of the 5-year Global COE Program “Center of Education and Research for Information Electronics Systems (2007–2011), awarded by the Ministry of Education, Culture, Sports, Science and Technology of Japan. From October 1984 to September 1985, he was a United Kingdom SERC Visiting Research Fellow in the Department of Electrical Engineering and Electronics at Liverpool University. He is an IEICE Fellow and was a co-recipient of the IEICE Transactions best paper of the year award 1996, 1998, and 2009 and also a recipient of Achievement award 2003. He is an IEEE Fellow and was a co-recipient of the IEEE Vehicular Technology Transactions best paper of the year award 1980 and again 1990 and also a recipient of Avant Garde award 2000. He was a recipient of Thomson Scientific Research Front Award 2004, Ericsson Telecommunications Award 2008, Telecom System Technology Award 2009, and Prime Minister Invention Prize 2010.